

Regular Article - Experimental Physics

Instrumental uncertainties in radiative corrections for the MUSE experiment

L. Li¹, S. Strauch^{1,a}, J. C. Bernauer^{2,3}, W. J. Briscoe⁴, A. Christopher Ndukwe⁵, E. Cline², D. Cohen⁶, K. Deiters⁷, E. J. Downie⁴, I. P. Fernando^{5,8}, A. Flannery¹, R. Gilman⁹, Y. Ilieva¹, M. Kohl⁵, I. Lavrukhin^{4,10}, W. Lin⁹, W. Lorenzon¹⁰, S. Lunkenheimer¹⁰, P. Mohanmurthy¹³, J. Nazeer⁵, M. Nicol¹, T. Patel⁵, A. Prosnyakov⁶, H. Reid¹⁰, P. E. Reimer¹¹, G. Ron⁶, T. Rostomyan⁷, O. M. Ruimi⁶, N. Sparveris¹², D. Yaari⁶

- ¹ Department of Physics and Astronomy, University of South Carolina, Columbia, SC 29208, USA
- ² Department of Physics and Astronomy, Stony Brook University, Stony Brook, NY 11794, USA
- ³ RIKEN BNL Research Center, Brookhaven National Laboratory, Upton, NY 11973, USA
- ⁴ Department of Physics, The George Washington University, Washington, DC 20052, USA
- ⁵ Department of Physics, Hampton University, Hampton, VA 23668, USA
- ⁶ Racah Institute of Physics, The Hebrew University of Jerusalem, 91904 Jerusalem, Israel
- ⁷ Paul Scherrer Institute, 5232 Villigen, Switzerland
- ⁸ Department of Physics, University of Virginia, Charlottesville, VA 22904, USA
- ⁹ Department of Physics and Astronomy, Rutgers, The State University of New Jersey, Piscataway, NJ 08854, USA
- ¹⁰ Randall Laboratory of Physics, University of Michigan, Ann Arbor, MI 48109, USA
- ¹¹ Physics Division, Argonne National Laboratory, Lemont, IL 60439, USA
- ¹² Department of Physics, Temple University, Philadelphia, PA 19122, USA
- ¹³ Laboratory for Nuclear Science, Massachusetts Institute of Technology, Cambridge, MA 02139, USA

Received: 13 July 2023 / Accepted: 8 December 2023 / Published online: 10 January 2024

© The Author(s), under exclusive licence to Società Italiana di Fisica and Springer-Verlag GmbH Germany, part of Springer Nature 2024

Communicated by Klaus Peters

Abstract The MUSE experiment at the Paul Scherrer Institute is measuring elastic lepton-proton scattering cross sections in a four-momentum transfer range from Q^2 of approximately 0.002–0.08 GeV² using positively and negatively charged electrons and muons. The extraction of the Born cross sections from the experimental data requires radiative corrections. Estimates of the instrumental uncertainties in those corrections have been made using the ESEPP event generator. The results depend in particular on the minimum lepton momentum that contributes to the experimental cross section and the fraction of events with hard initial-state radiation that is detected in the MUSE calorimeter and is excluded from the data. These results show that the angular-dependent instrumental uncertainties in radiative corrections to the electron cross section are less than 0.4% and are negligible for the muon cross section.

1 Introduction

The MUon Scattering Experiment (MUSE) at the Paul Scherrer Institute (PSI) [1,2] has been developed to measure elastic electron-proton and muon-proton scattering cross sections

For each beam momentum, electron and muon scattering cross sections, $(d\sigma/d\Omega_\ell)_{\rm exp}$, will be obtained as a function of the lepton scattering angle. The extraction of the electromagnetic form factors from the measured cross sections will use an iterative approach to match simulated and measured count rates. Radiative effects can be quantified by a correction factor $(1+\delta)$, which is defined in the relation between the measured experimental cross section and the Born cross section [3]

$$\left(\frac{d\sigma}{d\Omega_{\ell}}\right)_{\exp} = \left(\frac{d\sigma}{d\Omega_{\ell}}\right)_{\text{Born}} (1+\delta). \tag{1}$$

of positively and negatively charged leptons. Measurements are done at beam momenta p_0 of 115 MeV/c, 161 MeV/c, and 210 MeV/c and over a wide range of scattering angles θ between 20° and 100°. MUSE covers four-momentum-transfers from Q^2 of approximately 0.002–0.08 GeV². Each of the four data sets, $e^{\pm}p$ and $\mu^{\pm}p$, allows the extraction of the proton charge radius. In combination, the data test possible differences between the electron and muon interactions and two-photon exchange effects.

^a e-mail: strauch@sc.edu (corresponding author)

8 Page 2 of 7 Eur. Phys. J. A (2024) 60:8

The radiative correction accounts for higher-order processes, such as the dominant first-order bremsstrahlung process $\ell p \to \ell' p \gamma$, the vacuum polarization correction, the vertex corrections, and the two-photon-exchange corrections. It is estimated from model calculations of the Born and bremsstrahlung, $d\sigma_{\rm brems}$, cross sections in the kinematic settings of the experiment. Monte-Carlo simulations are used to carry out the integration of the bremsstrahlung cross section

$$\left(\frac{d\sigma}{d\Omega_{\ell}}\right)_{\rm exp} = \int_{p'_{\ell}} \int_{\Omega_{\gamma}} \frac{d\sigma_{\rm brems}}{d\Omega_{\ell} d\Omega_{\gamma} dp'_{\ell}} d\Omega_{\gamma} dp'_{\ell}, \tag{2}$$

where p_ℓ' is the momentum of the scattered lepton, and Ω_ℓ and Ω_γ are the solid angles of the incident lepton and final-state photon, respectively. The limits in the integration reflect the experimental conditions. The kinematics, event selection, lepton, and photon angular and momentum acceptances, detector resolutions, and functional behavior of the form factors will thus affect the size of the radiative corrections.

Dedicated calculations of radiative corrections for MUSE have been performed by Afanasev and collaborators [4–6], by Myhrer and collaborators in the framework of the Heavy Baryon Chiral Perturbation Theory [7,8], and within the McMule framework using the higher-order QED calculations [9, 10]. Second-order radiative corrections have also been calculated for MUSE in Ref. [11]. Two-photon exchange effects in MUSE kinematical region were studied by Tomalak and Vanderhaeghen [12–15] in the dispersion relation approach, by Weiss and collaborators [16] in the framework of Dispersively Improved Chiral Effective Field Theory, and by Paz and collaborators [17] using QED-NRQED effective field theory. However, the simulations to perform the integral in Eq. (2) require a suitable event generator, which, in the case of MUSE, must fulfill several requirements. First, the event generator needs to include the emission of a hard radiated photon in the initial and final state, which is beyond the soft-photon approximation. MUSE includes a large fraction of the radiative tail in the momentum acceptance. The hard photon needs to be propagated in the full Monte Carlo simulation. Second, the event generator needs to include the mass of the leptons to avoid the $Q^2 \gg m^2$ approximation in the calculation. The Elastic Scattering of Electrons and Positrons on Protons (ESEPP) event generator [3] takes into account the first-order radiative corrections of elastic scattering of charged leptons $(e^{\pm} \text{ and } \mu^{\pm})$ on protons and fulfills these requirements. We have used ESEPP with the Kelly parametrization of the proton form factors [18] for the present studies. Other generators that are viable for MUSE include those discussed in Refs. [19,20], and were found to give results in good agreement with those from ESEPP when run under similar conditions.

This paper presents a study of how the instrumental characteristics of the MUSE experiment impact the determination of radiative corrections. The details of the Monte Carlo sim-

ulation and the properties of detectors related to the radiative corrections will be presented. Results of the radiative corrections and their uncertainties from preliminary instrumental input to the model calculations will be discussed.

2 Experiment

2.1 Setup

Figure 1 shows a schematic layout of the experimental setup of MUSE in the π M1 sary beamline [21] at PSI.

The particle beam contains a mix of electrons, muons, and pions with a beam flux up to 3.5 MHz in the experiment. These particles go through the Beam Hodoscope (BH) detector for timing and particle identification [22]. The BH also measures the beam fluxes. Three Gas Electron Multiplier (GEM) chambers [23] determine the incident particle track. A veto detector suppresses triggers from off-axis particles. The target chamber contains a ladder with liquid-hydrogen, empty-cell, and solid targets, in addition to a non-target position [24]. Scattered particles are detected by two symmetric spectrometers, each with two Straw-Tube Tracker (STT) chambers and two planes of fast Scattered Particle Scintillators (SPS). The combined information from the GEM and STT trackers allow for the reconstruction of the vertex and scattering angle for the ep or μp reaction. The scatteringangular resolution for one event is dominated by multiple scattering and is smaller than 20 mrad. Systematic uncertainties of the scattering angle reconstruction are expected to be below $\sigma_{\theta} = 1$ mrad. The two SPS planes (front-wall and rear-wall) provide the scattered-particle event trigger which requires a hit in each scintillator wall. The unscattered particles pass the Beam Monitor (BM). The time-of-flight (TOF) from the BH to the SPS determines the reaction type (muon scattering vs. muon decay in flight). The TOF from the BH to the BM determines μ and π beam momenta. Channel beam momenta have been verified with those measurements to within $\sigma_{p_0}/p_0 = 0.2 \%$ [21]. The BM can also be used to suppress background from Møller and Bhabha scattering. The most downstream beamline detector is the calorimeter. It consists of 64 lead-glass blocks in a square arrangement 139 cm downstream of the target. The blocks have a size of $4 \text{ cm} \times 4 \text{ cm} \times 30 \text{ cm}$. The calorimeter is used to detect photons in the beam direction.

Particularly important for the determination of the radiative corrections are the lepton-detection threshold in the SPS detectors and the hard photon detection in the calorimeter.

2.2 Event selection

The magnitude of the momentum of the final-state lepton is not directly measured in MUSE. Instead, all scattered lep-



Eur. Phys. J. A (2024) 60:8 Page 3 of 7 8

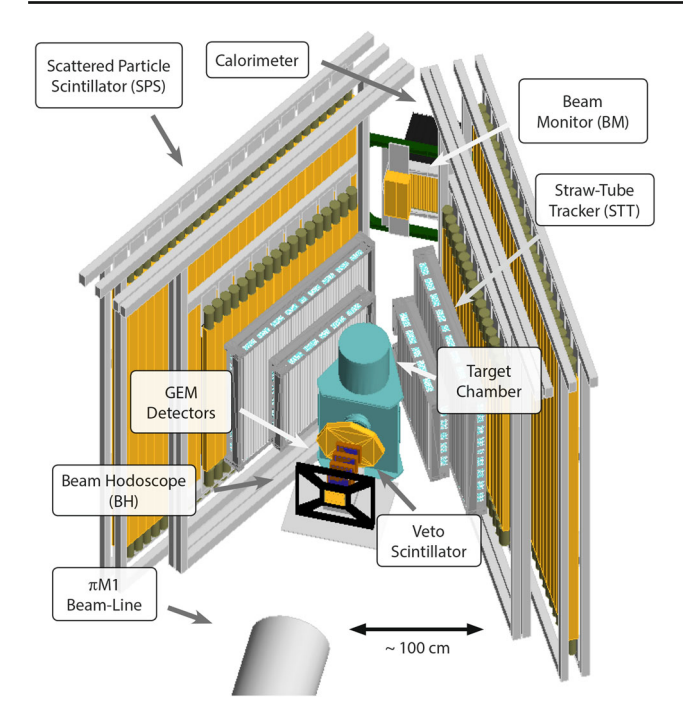


Fig. 1 Sketch of the MUSE experimental setup at the $\pi M1$ beamline at PSI as implemented in the MUSE Geant4 simulation

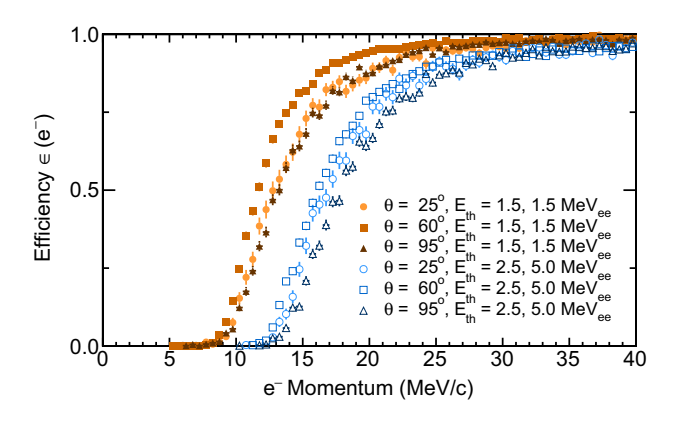


Fig. 2 Geant4 simulation of the electron detection threshold of the MUSE SPS detector. The efficiency of particle detection is shown as a function of momentum for various scattering angles and low (full symbols) and high (open symbols) light-output thresholds. The light-output thresholds $E_{\rm th}$ are given for the front and rear-walls separately

tons, from the threshold, $p'_{\ell, \min}$, to the elastic endpoint are included in the experimental yield. The threshold momentum depends on the scintillator light output and the discrimination thresholds set in the front- and rear-wall detectors of the SPS. A Geant4 simulation of the electron detection efficiency, $\epsilon(p'_e)$, is shown in Fig. 2.

The full symbols are for light output thresholds of $1.5~\text{MeV}_{ee}$ for each of the front and rear walls. The open symbols are for higher threshold values of $2.5~\text{MeV}_{ee}$ and $5.0~\text{MeV}_{ee}$ in the two walls, respectively. Particles with a scattering angle of about 60° traverse the walls approximately perpendicularly. Smaller or larger scattering angles result in higher momentum thresholds, as shown in Fig. 2, due to the larger path length in the scintillation material and related larger energy losses in the front wall. At very low momenta the lepton stops in the front wall, or deposits insufficient energy for the light output to be above the discriminator threshold.

The effective minimum momentum threshold, p'_{\min} , was determined to be the momentum value for which the integral of the bremsstrahlung cross section over the detection range from p'_{\min} to the endpoint, p'_{\max} , matches the efficiency weighted integral over all momenta

$$\int_{p'_{\min}}^{p'_{\max}} \frac{d\sigma_{\text{brems}}}{d\Omega_{\ell} d\Omega_{\gamma} dp'_{\ell}} d\Omega_{\gamma} dp'_{\ell}
= \int_{0}^{p'_{\max}} \epsilon(p'_{\ell}) \frac{d\sigma_{\text{brems}}}{d\Omega_{\ell} d\Omega_{\gamma} dp'_{\ell}} d\Omega_{\gamma} dp'_{\ell}.$$
(3)

We have evaluated Eq. (3) using $\epsilon(p'_\ell)$ from Fig. 2 and the ESEPP event generator for $\sigma_{\rm brems}$. The momentum threshold is a function of the discriminator thresholds in the SPS, the lepton scattering angle, and details of the event selection, e.g., cuts on the bremsstrahlung photons. For electrons and detection thresholds of 2.0 MeV_{ee} in both walls, it is about $p'_{\rm min}=14$ MeV/c, and for muons about $p'_{\rm min}=84$ MeV/c. We estimate the uncertainty of the threshold values to be $\sigma_{p',n}=2$ MeV/c.

 $\sigma_{p'_{\min}} = 2 \text{ MeV/}c.$ Photon production is often ignored in the experimental yield in electron-scattering experiments, and the bremsstrahlung cross section is integrated over the full solid angle of the real photons in the evaluation of radiative corrections. However, as shown below in Sect. 4, uncertainties in the radiative corrections in MUSE can be reduced when hard photons in the forward direction are excluded in the cross section. As an example of the anticipated MUSE calorimeter response, Fig. 3 shows the reconstructed photon momentum distribution for the scattering of 161 MeV/c electrons at 60° as a red histogram. The simulation is based on the ESEPP event generator. It includes the geometrical acceptance of the 8 × 8 calorimeter blocks, and the energy-dependent detector resolution. The parameterization of the resolution was tuned to experimental data with electron-beam momenta in the range from 20 MeV/c to 230 MeV/c. When the calorimeter is used to suppress initial-state radiation, only events with a reconstructed photon energy less than a specified energy cut are used in the subsequent analysis. For example, the green histograms in Fig. 3 display the accepted data with photon energies less than 80 %, 40 %, and 20 % of the beam energy.



¹ The electron light-output function of the SPS plastic scintillators is very nearly linear, and has been calibrated with photon sources following the method of Ref. [25]. The light output is reported in units of MeV electron equivalent (MeV_{ee}).

B Page 4 of 7 Eur. Phys. J. A (2024) 60:8

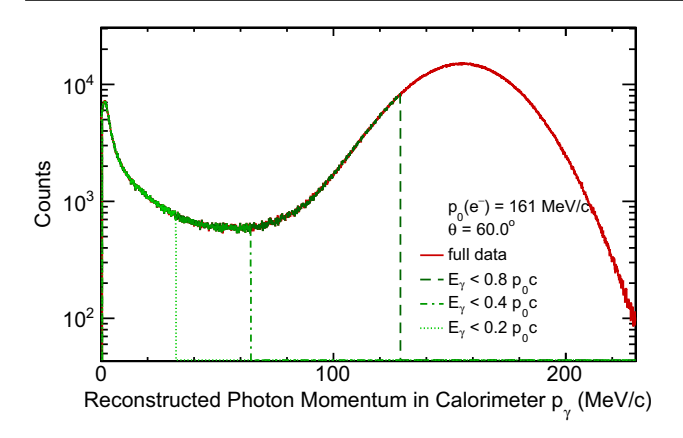


Fig. 3 Simulation of the reconstructed photon momentum in the MUSE calorimeter (red histogram) for scattering of 161 MeV/c electrons at 60°

Preliminary commissioning data show a relative energy resolution of the calorimeter of 20 %, at the energy corresponding to about half the beam momentum of 210 MeV/c, up to 25 % for 115 MeV/c. We assume the uncertainty of the *mean* of the reconstructed photon-energy to be better than $\sigma_{E_{\gamma}} = 5$ MeV.

3 Simulations of the lepton-scattering cross section

Figure 4 shows histograms from ESEPP simulations of the electron (red) and muon (blue) scattering cross sections at a kinematic setting with an incident beam momentum of $p_0 = 161 \text{ MeV}/c$ and scattering angle θ of 60°. This setting is at the center of the momentum and angular range of the experiment.

In the experiment, all scattered particles above the momentum detection threshold p'_{min} contribute to the experimental yield. The momentum ranges are indicated by the horizontal lines. Each histogram shows the elastic peak at high momentum and its radiative tail. The muon elastic peak is slightly offset from the electron peak due to the larger proton recoil energy in μp scattering. The apparent gap between the elastic peak and the tail is an artifact of the ESEPP calculation. The event generator includes explicitly hard bremsstrahlung photons in the tail region with energies as low as the cut-off energy $E_{\gamma}^{\rm cut}$. The contribution to the cross section from photons with $E_{\gamma} < E_{\gamma}^{\rm cut}$ is integrated over all photon directions and energies and is included in the elastic peak [3]. Due to their small mass, the cross section in the radiative tail is much larger for electrons than muons. In this kinematic setting, the cross section for ep at the e detection threshold is about 200 times larger than for μp at the μ threshold. The $\ell p \to \ell' p \gamma$ cross section vanishes for both lepton species as the scattered-lepton momentum reaches zero. The local maximum in the electron radiative tail at low final-state electron momenta is caused by the increase of the ep scattering cross section after initial-state photon emission from

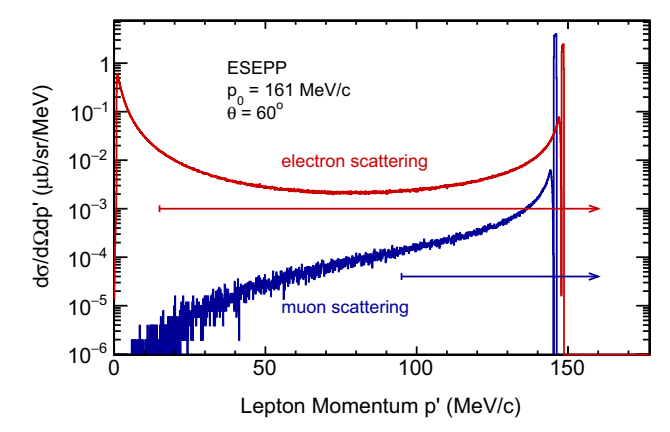


Fig. 4 ESEPP calculations of the electron (red) and muon (blue) scattering cross sections for an incident beam momentum of 161 MeV/c and a scattering angle of 60°. The cross sections are integrated over all final-state photon directions. The horizontal lines indicate the lepton-momentum acceptance of MUSE

the electron in the beam direction and the subsequent reduction of the electron momentum and momentum transfer in the scattering process [7].

4 Radiative corrections

We have used the ESEPP event generator in a simplified simulation of MUSE and studied the radiative corrections δ in a variety of experimental conditions. The simulation is simplified in that it is not a full simulation of the MUSE apparatus but assumes the nominal beam momentum, scattering angle, momentum-detection threshold, and photon calorimeter geometrical acceptance and energy reconstruction. Processes accompanying the passage of incident and outgoing particles through the upstream detector and target materials have not yet fully been considered. Initial tests with a more comprehensive simulation show that this simple approach encompasses all relevant effects and the two approaches give quantitatively similar results. Uncertainties in the beam momentum and scattering angle are so small that they do not significantly contribute to the uncertainty in the radiative corrections. The uncertainty in the minimum lepton momentum p'_{\min} , however, contributes strongly to radiative corrections in electron scattering but not in muon scattering.

This result is exemplified in the values for δ that are shown in Fig. 5 as a function of p'_{\min} for electron (top panel) and muon (bottom panel) beams of a momentum of 161 MeV/c and for a mid-range scattering angle of 60°. The correction parameter δ is negative when the scattering cross section is smaller than the Born cross section at high values of p'_{\min} .

The red curves show the results for all scattering events, regardless of the emission of photons. For ep, the full result shows a strong dependence on p'_{\min} with a steep slope



Eur. Phys. J. A (2024) 60:8 Page 5 of 7 8

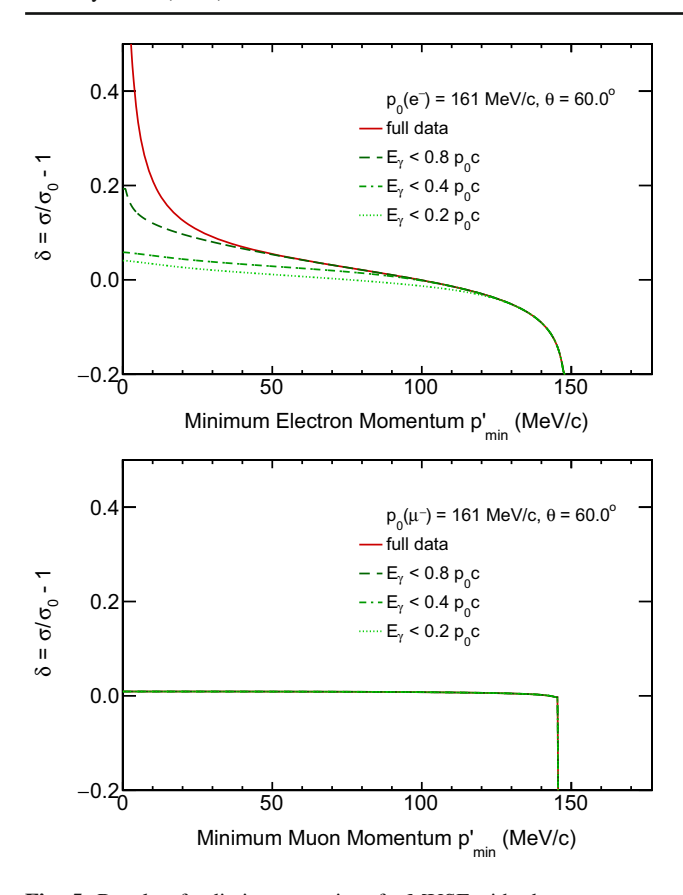


Fig. 5 Results of radiative corrections for MUSE with a beam momentum of $161 \, \text{MeV/}c$ and a scattering angle of 60° . The top panel shows the results for electron scattering, the bottom panel the results for muons. The curves show the results without (red) and with increasingly strong cuts on initial-state radiation using the calorimeter (green). Those distributions all overlap in the muon case

 $(\partial \delta/\partial p'_{\min} > 1\%$ per 1 MeV/c) close to the SPS detection threshold of about 14 MeV/c. If uncontrolled, the instrumental uncertainty in p'_{\min} would generate a considerable uncertainty in δ .

As discussed in Sect. 3, the increase in δ with a decrease in p'_{\min} is linked to the increase of the ep cross section with reduced beam momentum after the emission of high-energy initial-state radiation. The initial-state radiation is strongly forward peaked, and the MUSE calorimeter in the beamline downstream of the target is capable of detecting these bremsstrahlung photons. The various green curves in Fig. 5 show the results for δ after vetoing an increasing fraction of events with forward going hard photons. The lower the chosen photon-energy cut to suppress the initial-state radiation, the smaller are the radiative corrections and their dependence on p'_{\min} .

However, as seen in Fig. 3, a sizable fraction of the initial-state-radiation momentum distribution is at low photon momenta. Selecting the photon-energy cut in that region increases the uncertainty in the experimental cross section and in the corresponding radiative corrections due to uncer-

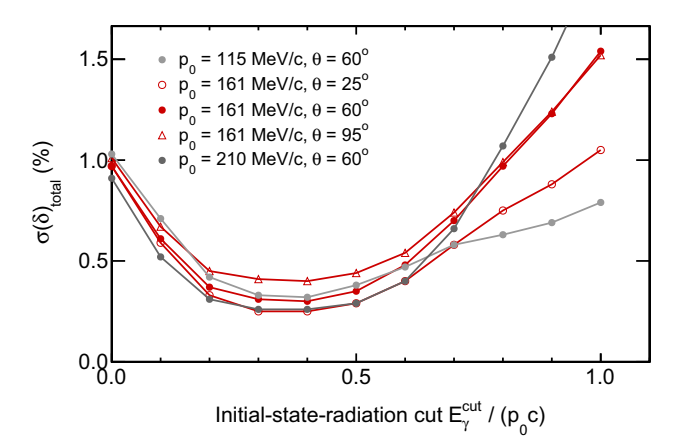


Fig. 6 Total uncertainties of radiative corrections σ_{δ} for ep scattering and various beam momenta and scattering angles in MUSE as a function of the photon-energy cut E_{γ}^{uv}

tainties in the reconstructed photon momentum. To determine the optimum event selection with the smallest overall uncertainty for the radiative corrections for ep, we repeated the simulations, systematically increasing the upper limit of the energies of the accepted hard-photons in the forward direction from 0 to 100% of the beam momentum.

The results are shown in Fig. 6. We found a shallow minimum of the total uncertainty with a photon energy cut of $E_{\gamma} < 0.4 p_0 c$. Radiative corrections for muons are much smaller than for electrons and nearly independent on p'_{\min} , as shown in the bottom panel of Fig. 5. Because there are not many photons emitted in the forward direction in the μp scattering process, the calorimeter cut does not significantly affect the data, and the results of all calculation variations overlap.

Table 1 summarises the radiative-correction values at the three MUSE beam momenta and for three scattering angles. The table also indicates the minimum lepton momentum that was used in the determination of the corrections for each scattering angle. The statistical uncertainties in the corrections are of the order 10^{-3} . Suppressing hard initial-state radiation using the photon calorimeter reduces the ep radiative corrections to the Born cross section by a factor of 2.5 to 6, depending on the kinematic setting, to values below 0.1. The corrections for μp scattering are at most 0.01 and independent of the calorimeter response.

The impact of the instrumental uncertainties in the key input parameters x_i of the calculation – the beam momentum, scattering angle, minimum final-state lepton momentum, and the photon-energy cut for forward going photons – was studied by varying that input to determine $\partial \delta/\partial x_i$ and propagate the experimental uncertainties into the uncertainty of the radiative corrections. The preliminary results for a calorimeter threshold of $E_{\gamma} < 0.4 p_0 c$ are given in Table 2 for ep scattering.



8 Page 6 of 7 Eur. Phys. J. A (2024) 60:8

Table 1 Radiative corrections δ for MUSE. Values are given for ep and μp scattering at various kinematic settings and for fully integrated final-state bremsstrahlung photons (full data) and after suppression of

photons in the beam direction with the calorimeter $(E_{\gamma} < 0.4 p_0 c)$. The statistical uncertainties in the corrections are of the order 10^{-3}

$p_0 \text{ (MeV/}c)$	115 25°	115 60°	115 95°	161 25°	161 60°	161 95°	210 25°	210 60°	210 95°
ep									
$p'_{e,\min}$ (MeV/c)	14.8	13.0	14.4	14.8	13.0	14.4	14.8	13.0	14.4
δ_e (full data)	0.091	0.119	0.119	0.130	0.173	0.172	0.173	0.239	0.235
$\delta_e \left(E_{\gamma} < 0.4 p_0 c \right)$	0.026	0.042	0.049	0.028	0.049	0.060	0.030	0.056	0.070
μp									
$p'_{\mu, \min}$ (MeV/c)	84.2	82.4	85.8	84.2	82.4	85.8	84.2	82.4	85.8
δ_{μ} (full data)	0.001	0.005	0.003	0.004	0.009	0.008	0.006	0.010	0.010
$\delta_{\mu} \left(E_{\gamma} < 0.4 p_0 c \right)$	0.001	0.005	0.003	0.004	0.009	0.008	0.006	0.010	0.010

Table 2 Uncertainties of radiative corrections σ_{δ} for ep scattering in MUSE, including the various contributions from the experimental uncertainties in the model input parameters p_0 , θ_e , p'_{\min} , and E_{ν} . The

values assume a cut on hard photons with $E_{\gamma} > 0.4 p_0 c$ in the MUSE calorimeter. The total uncertainty does not include model uncertainties in ESEPP

	,									
$p_0 \text{ (MeV/}c)$	115 25°	115 60°	115 95°	161 25°	161 60°	161 95°	210 25°	210 60°	210 95°	
$ (\partial \delta_e/\partial p_0)\sigma_{p_0} $	0.01%	0.01%	0.00%	0.01 %	0.00%	0.00%	0.00%	0.03 %	0.01 %	
$ (\partial \delta_e/\partial \theta_e)\sigma_{\theta_e} $	0.00%	0.00%	0.00%	0.00%	0.00%	0.00%	0.00%	0.00%	0.00%	
$ (\partial \delta_e/\partial p'_{\min})\sigma_{p'_{\min}} $	0.05%	0.18%	0.30%	0.03 %	0.16%	0.31 %	0.02%	0.13 %	0.31 %	
$ (\partial \delta_e/\partial E_{\gamma})\sigma_{E_{\gamma}} $	0.32%	0.33 %	0.33 %	0.25 %	0.26 %	0.26%	0.20 %	0.22%	0.22 %	
σ_{δ_e}	0.32%	0.38%	0.45 %	0.25 %	0.30 %	0.40 %	0.20%	0.26 %	0.38 %	

Experimental uncertainties in the beam momentum and scattering angle are too small to affect the radiative corrections significantly. Contributions to the uncertainty budget from the photon-energy cut in the calorimeter are independent of the scattering angle and decrease from about 0.33-0.22 % with increasing beam momentum. Those uncertainties do contribute to the absolute cross section normalization uncertainty but do not contribute to the uncertainty of the extraction of the proton charge radius which relies on the analysis of the slope of the cross section. Uncertainties in the knowledge of the electron detection threshold, and thus the lower bound in the integration of Eq. (2), affect the cross section angular distribution. The contribution to the uncertainty in the radioactive correction is small at forward angles and about 0.3% at backward angles. For μp scattering, there are no significant contributions to the uncertainty of radiative corrections from experimental input parameters to the model calculations. The estimated uncertainties of the radiative corrections for $e^+(\mu^+)$ scattering is similar to $e^-(\mu^-)$ within the statistical precision of our simulations. The results in Table 2 are based on the Kelly parametrization of the proton form factors. Simulations with the Dipole form factor lead to identical results in the estimated uncertainties. Other model uncertainties for ep and μp scattering, like higherorder corrections to the cross sections, are estimated to have

minimal effect on the assessment of the *instrumental* uncertainties in the radiative corrections and are not included in this study. Work is underway to improve the detector calibrations and simulations for the SPS and calorimeter detectors to help reducing instrumental uncertainties in p'_{\min} and E_{γ} , and to minimize MUSE systematic uncertainties.

5 Summary

MUSE is a high-precision experiment to measure the proton charge radius, study possible two-photon exchange mechanisms, and have a direct μ/e comparison of the elastic cross sections. Without a magnetic spectrometer, MUSE does include a wide range of the final-state lepton momenta in the experimental yield. A dedicated downstream photon detector helps to suppress initial-state radiation effects, and, in turn, reduce instrumental uncertainties to the radiative corrections. Simplified Monte Carlo simulations with the ESEPP event generator show that the radiative corrections δ to the Born cross section are below 0.1 for ep and 0.01 for μp scattering. The total uncertainties of the radiative corrections from the uncertainties in the experimental inputs for electron scattering are smaller than 0.5%, including angular dependent contributions that are related to the proton radius extraction, of up to about 0.3 %. The total uncertainties of the radiative



Eur. Phys. J. A (2024) 60:8 Page 7 of 7 8

corrections from the uncertainties in the experimental input for muons are negligible.

Acknowledgements The work was supported by the U.S. National Science Foundation grants PHY-2111050, PHY-2012144, PHY-1812402, PHY-2110229, PHY-2012940, PHY-1505934, PHY-1812402, PHY-2113436, PHY-2209348, PHY-1913653 and HDR-1649909; the U.S. Department of Energy grants DE-SC0012485, DE-SC0016577, DE-AC02-06CH11357, and DE-SC0012589; the Paul Scherrer Institute; and the US-Israel Binational Science Foundation. It was also supported by Sigma Xi grants G2017100190747806 and G2019100190747806.

Data Availability Statement This manuscript has no associated data or the data will not be deposited. [Authors' comment: The data supporting the findings of this study are available within the article. These data were derived from resources available at https://github.com/gramolin/esepp.]

References

- 1. R. Gilman, et al., Technical design report for the Paul Scherrer Institute Experiment R-12-01.1: studying the proton "Radius" puzzle with μp elastic scattering (2017). arXiv:1709.09753 [physics.insdet]
- E. Cline, J. Bernauer, E.J. Downie, R. Gilman, MUSE: the MUon scattering experiment. SciPost Phys. Proc. 5, 023 (2021). https:// doi.org/10.21468/SciPostPhysProc.5.023
- A.V. Gramolin, V.S. Fadin, A.L. Feldman, R.E. Gerasimov, D.M. Nikolenko, I.A. Rachek, D.K. Toporkov, A new event generator for the elastic scattering of charged leptons on protons. J. Phys. G41(11), 115001 (2014). https://doi.org/10.1088/0954-3899/41/11/115001. arXiv:1401.2959 [nucl-ex]
- A. Afanasev, A. Ilyichev, Radiative corrections to the lepton current in unpolarized elastic lp-interaction for fixed Q² and scattering angle. Eur. Phys. J. A 57(9), 280 (2021). https://doi.org/10.1140/ epja/s10050-021-00582-w. arXiv:2106.11103 [hep-ph]
- O. Koshchii, A. Afanasev, Charge asymmetry in elastic scattering of massive leptons on protons. Phys. Rev. D 96(1), 016005 (2017). https://doi.org/10.1103/PhysRevD.96.016005. arXiv:1705.00338 [nucl-th]
- A. Afanasev, A. Ilyichev, Contribution of hard photon emission to the charge asymmetry in elastic lepton- and antilepton-proton scattering. Phys. Rev. D 105(1), 011301 (2022). https://doi.org/10. 1103/PhysRevD.105.L011301. arXiv:2007.02087 [hep-ph]
- P. Talukdar, F. Myhrer, G. Meher, U. Raha, Low-energy leptonproton bremsstrahlung via effective field theory. Eur. Phys. J. A 54(11), 195 (2018). https://doi.org/10.1140/epja/i2018-12629-8. arXiv:1810.04027 [nucl-th]
- P. Talukdar, V.C. Shastry, U. Raha, F. Myhrer, Lepton-proton two-photon exchange in chiral perturbation theory. Phys. Rev. D 101(1), 013008 (2020). https://doi.org/10.1103/PhysRevD.101. 013008. arXiv:1911.06843 [nucl-th]
- Y. Ulrich, McMule-QED Corrections for Low-Energy Experiments. Ph.D. thesis, Zurich U., Inst. Math. (2020)
- P. Banerjee, T. Engel, A. Signer, Y. Ulrich, QED at NNLO with McMule. SciPost Phys. 9, 027 (2020). https://doi.org/10.21468/ SciPostPhys.9.2.027 arXiv:2007.01654 [hep-ph]
- R.-D. Bucoveanu, H. Spiesberger, Second-order leptonic radiative corrections for lepton-proton scattering. Eur. Phys. J. A 55(4), 57 (2019). https://doi.org/10.1140/epja/i2019-12727-1. arXiv:1811.04970 [hep-ph]

O. Tomalak, M. Vanderhaeghen, Two-photon exchange corrections in elastic muon-proton scattering. Phys. Rev. D 90(1), 013006 (2014). https://doi.org/10.1103/PhysRevD.90.013006. arXiv:1405.1600 [hep-ph]

- O. Tomalak, M. Vanderhaeghen, Two-photon exchange correction to muon-proton elastic scattering at low momentum transfer. Eur. Phys. J. C 76(3), 125 (2016). https://doi.org/10.1140/epjc/s10052-016-3966-3. arXiv:1512.09113 [hep-ph]
- O. Tomalak, Two-photon exchange correction in elastic leptonproton scattering. Few Body Syst. 59(5), 87 (2018). https://doi. org/10.1007/s00601-018-1413-8. arXiv:1806.01627 [hep-ph]
- O. Tomalak, M. Vanderhaeghen, Dispersion relation formalism for the two-photon exchange correction to elastic muon-proton scattering: elastic intermediate state. Eur. Phys. J. C 78(6), 514 (2018). https://doi.org/10.1140/epjc/s10052-018-5988-5. arXiv:1803.05349 [hep-ph]
- F. Gil-Domínguez, J.M. Alarcón, C. Weiss, Proton charge radius extraction from muon scattering at MUSE using dispersively improved chiral effective field theory (2023). arXiv:2306.01037 [hep-ph]
- S.P. Dye, M. Gonderinger, G. Paz, Elements of QED-NRQED effective field theory: II. Matching of contact interactions. Phys. Rev. D 100(5), 054010 (2019). https://doi.org/10.1103/PhysRevD. 100.054010. arXiv:1812.05056 [hep-ph]
- J.J. Kelly, Simple parametrization of nucleon form factors. Phys. Rev. C 70, 068202 (2004). https://doi.org/10.1103/PhysRevC.70. 068202
- I. Akushevich, O.F. Filoti, A.N. Ilyichev, N. Shumeiko, Monte Carlo generator ELRADGEN 2.0 for simulation of radiative events in elastic ep-scattering of polarized particles. Comput. Phys. Commun. 183, 1448–1467 (2012). https://doi.org/10.1016/j.cpc.2012. 01.015. arXiv:1104.0039 [hep-ph]
- J.C. Bernauer, Electric and magnetic form factors of the proton. Phys. Rev. C 90(1), 015206 (2014). https://doi.org/10.1103/ PhysRevC.90.015206. arXiv:1307.6227 [nucl-ex]
- E. Cline, Characterization of muon and electron beams in the Paul Scherrer Institute PiM1 channel for the MUSE experiment. Phys. Rev. C 105(5), 055201 (2022). https://doi.org/10.1103/PhysRevC. 105.055201. arXiv:2109.09508 [physics.ins-det]
- T. Rostomyan, Timing detectors with SiPM read-out for the MUSE experiment at PSI. Nucl. Instrum. Methods A 986, 164801 (2021). https://doi.org/10.1016/j.nima.2020.164801. arXiv:2007.12207 [physics.ins-det]
- A. Liyanage, M. Kohl, J. Nazeer, T. Patel, Development of GEM detectors at Hampton University. PoS MPGD2017, 026 (2019). https://doi.org/10.22323/1.322.0026. arXiv:1803.00132 [physics.ins-det]
- P. Roy, A liquid hydrogen target for the MUSE experiment at PSI. Nucl. Instrum. Methods A 949, 162874 (2020). https://doi.org/10. 1016/j.nima.2019.162874. arXiv:1907.03022 [physics.ins-det]
- G. Dietze, H. Klein, Gamma-calibration of NE 213 scintillation counters. Nucl. Instrum. Methods Phys. Res. 193(3), 549–556 (1982). https://doi.org/10.1016/0029-554X(82)90249-X

Springer Nature or its licensor (e.g. a society or other partner) holds exclusive rights to this article under a publishing agreement with the author(s) or other rightsholder(s); author self-archiving of the accepted manuscript version of this article is solely governed by the terms of such publishing agreement and applicable law.

